Ground state and vortex structure of the $N=5$ and $N=6$ electron quantum dot

M. B. Tavernier,[1,*] E. Anisimovas,[2,†] and F. M. Peeters[1,‡]
[1]*Departement Fysica, Universiteit Antwerpen, Groenenborgerlaan 171, B-2020 Antwerpen, Belgium*
[2]*Semiconductor Physics Institute, Goštauto 11, LT-01108 Vilnius, Lithuania*
(Received 15 March 2006; published 13 September 2006)

A system of $N=5$ and 6 two-dimensional Coulomb-interacting electrons, trapped in a harmonic potential and subjected to a perpendicular magnetic field, is studied using an exact-diagonalization technique. The results are summarized in a phase diagram, indicating the ground state as a function of the magnetic field and the electron-electron interaction strength. The transformation to a Wigner crystal after the breakdown of the maximum density droplet is investigated and is related to the vortex structure of the different states. The internal structure of the composite fermion is investigated as function of the magnetic field and related to several properties of the quantum dot (e.g., compressibility, liquid or crystal, stability of the ground state, and so on).

DOI: 10.1103/PhysRevB.74.125305 PACS number(s): 73.21.La, 71.10.−w

I. INTRODUCTION

Vortices are ubiquitous in nature, with examples ranging from the Great Red Spot on Jupiter and hurricanes and tornadoes in the Earth atmosphere to rotating Bose-Einstein condensates. Vortices consist of a center and circulating matter and reflect formation of dynamically stable patterns in a turbulent environment. In quantum dots (and generally in condensed matter physics) we encounter vortices in the electronic wave function—they consist of a point where the electron density is zero and by walking in a small circle around it a jump of 2π will occur in the phase of the wave function. The importance of these vortices emerged after the discovery of the fractional quantum Hall effect.[1] In his attempt to describe the experimentally obtained results Laughlin localized vortices at the position of the electrons to form the Laughlin wave function[2]

$$\Psi = \prod_{j<k} (z_j - z_k)^{2p+1} \exp\left(-\frac{1}{4}\sum_l |z_l|^2\right), \tag{1}$$

which describes a system of N particles at filling factor $\nu = 1/(2p+1)$. The length is measured in units of the magnetic length $l_c=\sqrt{\hbar c/eB}$ and $z=x-iy$ is a complex number expressing the two-dimensional coordinates of the electrons in the plane. The Jastrow factor expresses a strong correlation between the vortices and the electrons and will help in separating the electrons from each other (and thus reducing the electron-electron repulsion energy). The relation between the filling factor ν and the angular momentum L is given by $\nu = N(N-1)/2L$.

The introduction of the composite fermion[3–5] as an effective new particle emphasized again that vortices play a crucial role in the system. This new particle consists of an electron that binds an even number of zeros (magnetic flux quanta) from the wave function to it, and thus is transformed into a weakly interacting quasiparticle moving in a reduced magnetic field (due to the partial cancellation of the magnetic field by the attached flux quanta). The fractional quantum Hall effect is then understood in terms of the integer quantum Hall effect for these new quasiparticles.

Before investigating the properties and behavior of vortices in quantum dots it is important to fully understand how the system behaves in an external magnetic field. Recent techniques have made it possible to create quantum dots with a few electrons trapped inside.[6–8] The nature of the confining potential depends on the experimental setup but often a harmonic potential is appropriate to model the system. The interplay of several effects inside the quantum dot (electron repulsion, spin effects, Zeeman interaction) makes this an interesting system to study, exhibiting ground-state transitions,[9–13] formation of Wigner crystals,[15] magic angular momenta,[16] and several other phenomena. When the number of electrons inside the quantum dot is small (typically $N \leqslant 6$) an exact diagonalization (ED) scheme is possible, as performed in Ref. 9 for systems with $N=5$ and 6. Systems with larger numbers of electrons can be studied when one restricts the basis functions to, e.g., the lowest Landau level (LLL), which significantly reduces the computing time. With approximate methods, like the Hartree-Fock method, renormalized perturbation series,[17,18] and approximate wave functions, like the Laughlin wave function and the rotating electron molecule wave function[19,20] (REM), a lot of results have been obtained in the past. The formation of vortices in few-electron quantum dots has recently been the subject of research.[21–24]

Here we will present a detailed study of systems of $N=5$ and 6 electrons, trapped in a harmonic potential and subject to a perpendicular magnetic field. For a system with six classical particles two configurations will emerge:[15] one with six electrons on a ring and the other with five on a ring and one in the center. It was suggested that the system tunnels between these two energy minima.[25] The competition between these different ground-state symmetries will lead to interesting features in the quantum-mechanical system. Since this is also a system with one electron in the center, one could expect the appearance of bulk effects. Special attention will be given to the vortex structure and its relation to several properties of the quantum dot like the compressibility and the radial density.

The structure of the paper is as follows. In Sec. II the theory of the involved computational methods is presented,

 ©2006 The American Physical Society

results for five electrons are described in Sec. III, and for six electrons in Sec. IV. We conclude in Sec. V.

II. MODEL

We model the system as N electrons moving in the $z=0$ plane and laterally trapped in a harmonic confining potential $V(r)=m^*\omega_0^2 r^2/2$ where m^* is the effective mass of the electrons in the host semiconductor, ω_0 is the oscillator frequency of the confining potential, and $\mathbf{r}=(x,y)$ denotes the position in the $z=0$ plane. To make optimal use of the circular symmetry of the problem, the vector potential will be expressed in the symmetric gauge $\mathbf{A}=B(-y,x,0)/2$. The Hamiltonian of this system is then given by

$$\hat{H}=\sum_{i=1}^{N}\left(\frac{\hat{\mathbf{p}}_i^2}{2m^*}+\frac{m^*\omega_0^2 r_i^2}{2}\right)+\sum_{i>j}^{N}\frac{e^2/\varepsilon}{|\mathbf{r}_i-\mathbf{r}_j|}+\sum_{i=1}^{N}\frac{1}{8}m^*\omega_c^2 r_i^2 - \frac{1}{2}\hbar\omega_c\hat{L}_z+\frac{1}{2}g^*\frac{m^*}{m_e}\hat{S}_z\hbar\omega_c, \tag{2}$$

where the last three terms represent the contribution due to the magnetic field with ω_c being the cyclotron frequency, g^* the effective g factor, m_e the bare electron mass, $\hat{L}_z$ the total projected angular momentum operator, and $\hat{S}_z$ the total projected spin operator. Since the latter two commute with the Hamiltonian we can work in subspaces of fixed L_z and S_z and the associated terms become constants while in these subspaces.

We study this system using dimensionless parameters,[26] i.e., measuring lengths in $l_0=\sqrt{\hbar/m^*\omega_0}$, the oscillator length, and energies in $\hbar\omega_0$. A dimensionless parameter $\lambda=l_0/a_B^*$ (here $a_B^*=\varepsilon\hbar^2/e^2m^*$ is the effective Bohr radius) describes the strength of the electron-electron interaction. The dimensionless Hamiltonian becomes

$$\hat{H}=\sum_{i=1}^{N}\left[-\frac{1}{2}\nabla_i^2+\frac{1}{2}\left(1+\frac{1}{4}\Omega_c^2\right)r_i^2\right]+\lambda\sum_{i>j}^{N}\frac{1}{|\mathbf{r}_i-\mathbf{r}_j|} + \frac{\Omega_c}{2}\left(g^*\frac{m^*}{m_e}S_z-L_z\right), \tag{3}$$

with $\Omega_c=\omega_c/\omega_0$.

The effect of an external applied magnetic field can be understood as a rescaling of $\mathbf{r}_i$ to $\alpha\mathbf{r}_i$, with $\alpha^4=1+\frac{1}{4}\Omega_c^2$. This results in a new effective $\lambda^*=\lambda/\alpha$ strength for the Coulomb interparticle interaction. This shows that to calculate the energies and wave functions at finite values of the magnetic field one simply needs to calculate these at $\Omega_c=0$ and with a modified λ. The terms with L_z and S_z can be simply added since we work in subspaces of fixed L_z and S_z.

The multiparticle wave function is expanded in a basis of Slater determinants constructed from the Fock-Darwin orbitals. The number of basis determinants that have to be included depends on the desired accuracy (e.g., for the construction of the phase diagrams for $N=5$ at $L=10$, 58 830 terms were used). For $N=5,6$ the computational demands increase dramatically when one increases the size of the basis used. Restricting the basis functions used to the LLL generally yields good results which are obtained within a reasonable time and is a very accurate approximation at high magnetic fields (and thus high angular momenta).

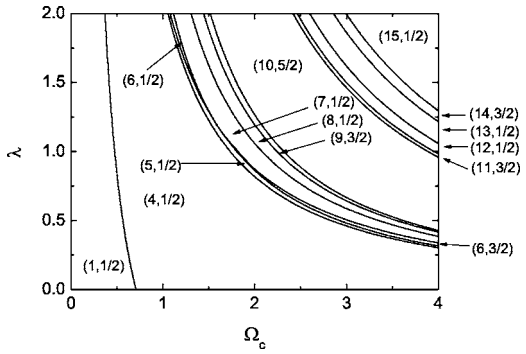

FIG. 1. Phase diagram showing the ground states for a system with $N=5$ electrons as a function of λ and Ω_c. Angular momenta up to 15 are included. The states are indicated as (L,S). Zeeman interaction is not included.

We complement the results obtained from the exact diagonalization by those given by the REM wave functions.[19,20] These functions are constructed by placing Gaussians at the classical positions of electrons in strong magnetic fields and a subsequent restoration of symmetry. For a small number of electrons ($N\leqslant 5$), the electrons crystallize into a single ring.[15] The resulting wave function with the angular momentum L reads[20]

$$\Psi_L=\sum_{0\leqslant l_1<l_2<\cdots<l_N}^{l_1+\cdots+l_N=L}\left(\prod_{j=1}^{N}l_j!\right)^{-1}\left[\prod_{1\leqslant j<k\leqslant N}\sin\left(\frac{\pi}{N}(l_j-l_k)\right)\right] \times\mathcal{D}(l_1,l_2,\ldots,l_N)\exp\left(-\sum_{j=1}^{N}z_j z_j^*/2\right). \tag{4}$$

Here, z_j denotes the complex electron coordinate measured in units of $l_c\sqrt{2}$ with $l_c=\sqrt{\hbar c/eB}$ being the magnetic length, and $\mathcal{D}$ is the Slater determinant

$$\mathcal{D}(l_1,l_2,\ldots,l_N)=\det[z_1^{l_1},z_2^{l_2},\ldots,z_N^{l_N}]. \tag{5}$$

The wave function describes spin-polarized states of angular momentum $L=L_0+Nm$ where $L_0=N(N-1)/2$ is the smallest possible angular momentum of N spin-polarized electrons in the lowest Landau level, and m is a non-negative integer. For a higher number of electrons (e.g., $N=6$) several rings can form and a slightly different form of the wave function is used (which for $N=6$ ensures that one electron is in the center of the dot).

III. RESULTS FOR FIVE ELECTRONS

By calculating the energies for all angular momenta and spin states we are able to construct a phase diagram showing the ground state in the (λ,Ω_c) plane. In what follows we will indicate the multiparticle ground states with (L,S) and the single-particle states with (n,l,s), where n, l, and s are the primary, angular, and spin quantum numbers, respectively. In Fig. 1 we show the ground states of a five-electron quantum

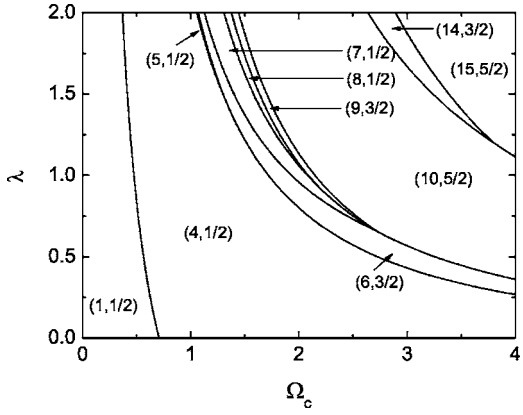

FIG. 2. Same as Fig. 1 but now with Zeeman interaction included.

dot without the Zeeman contribution. Figure 2 shows the same but with the Zeeman interaction included using GaAs parameters. The ground state at low magnetic fields is $(1,1/2)$ which is transformed into $(4,1/2)$ when the magnetic field is increased. Notice that the critical magnetic field needed for this transition depends only slightly on λ, which is an important difference between this transition and the other transitions that occur in the system. This can be understood when we look at the dominating Slater determinants, which are shown in Fig. 3. The electron in the $(0,-1,1/2)$ state will jump to the $(0,2,1/2)$ state due to the lowering of the positive angular momentum states by application of the magnetic field. The transition is therefore almost entirely induced by an increase of the magnetic field. In the subsequent transitions the electron repulsion will play a crucial role, and competition between the magnetic field and the electron repulsion will decide the ground state of the system. A similar transition was found earlier[26] in a four-electron quantum dot where the phase boundary originated from $(\lambda=0,\ \Omega_c=0)$. Afterward, through a series of transitions, the system evolves to the fully polarized maximum density droplet (MDD) state $(10,5/2)$. All angular momenta between the $(4,1/2)$ and $(10,5/2)$ states are accessed by the system. When the Zeeman interaction is turned on some of these states will be squeezed out at high magnetic fields as can be seen from Fig. 2. One last thing to note is the influence of the Zeeman interaction on the nature of the transitions leading to the MDD state. The Zeeman interaction will cause the different spin states to split in energy. Due to this splitting we find the transitions $(4,1/2)\rightarrow(6,3/2)\rightarrow(10,5/2)$ with increasing

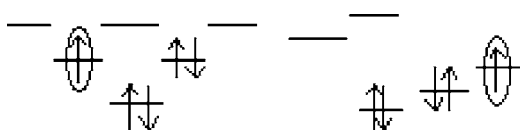

FIG. 3. The left-hand side shows the dominating Slater determinant for the $(1,1/2)$ state and the right-hand side that for the $(4,1/2)$ state for $N=5$ particles. The positive angular momenta are lowered in energy by the magnetic field while the opposite happens for the negative ones. This causes one electron to jump from the $(0,-1,1/2)$ state to the $(0,1,1/2)$ state.

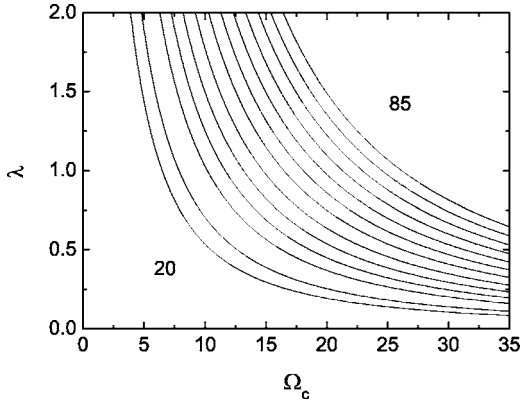

FIG. 4. The ground state at high magnetic fields. Full polarization of the spin was assumed and the exact diagonalization was limited to the LLL. Angular momenta from 20 to 85 are included in the calculation. Each transition corresponds to an increase of the angular momentum by 5.

magnetic field for $\lambda\rightarrow 0$, indicating that the electron repulsion is not the only driving mechanism. A similar effect was observed in the $N=4$ system and can be seen from Fig. 2 in Ref. 26 where one can observe the phase boundaries reaching the $\lambda=0$ line at certain Ω_c values for the transitions leading to the MDD state. The lowering of the energy of the positive angular momentum states by the magnetic field will cause the spin-down electrons to jump to those states. This means that for the case without Zeeman interaction the transition curves will asymptotically approach the $\lambda=0$ line as $\Omega_c\rightarrow\infty$.

When comparing our results to those of Ref. 9 we notice very good agreement between Fig. 2 and Fig. 1 in Ref. 9, keeping in mind that γ in Ref. 9 is inversely related to our λ.

Figure 4 shows the ground state as a function of λ and Ω_c for large angular momenta. Due to the long calculation times these calculations were restricted to the LLL and full polarization was assumed. One can see that the angular momentum goes in steps of 5. This result is expected taking the magic angular momentum theory[16] into account, which states that for a 5-0 symmetry (five electrons on a ring and none in the center) only states with angular momentum of multiples of five (counted from the MDD state) occur as ground states.

In Fig. 5 we plot the radial electron densities for several of the ground states. It can be clearly seen that for the $(1,1/2)$ and $(4,1/2)$ states the density is highest close to $r=0$. For $(6,3/2)$ the density flattens out and for $(10,5/2)$, the MDD state is formed, where the density forms a droplet as already discussed in numerous papers. On further increasing the angular momentum the MDD state breaks down and a minimum forms near $r=0$.

Figure 6 shows the pair-correlation function for several ground-state angular momenta ranging from 15 to 35. One can see clearly how the Wigner crystal appears as L increases. The electrons become more correlated and form a ring structure as in the classical system.[15]

By fixing the positions of all electrons but one in the multiparticle wave function, we can investigate the conditional electron wave function. Figure 7 shows the contour plots of the phase of the reduced wave function for several

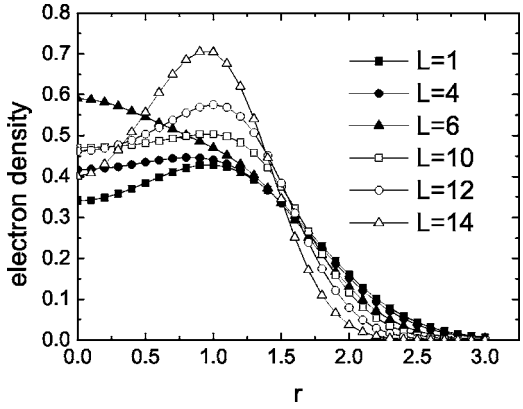

FIG. 5. Radial electron densities as a function of r, the distance from the center of the dot, at $\lambda=2$ for several ground states indicated as (L,S). The distance is measured in units of l_0. Notice how a minimum forms around $r=0$ for the states after the breakdown of the MDD state. The Zeeman interaction is not included.

angular momenta at which the system is fully polarized. Since there is no noticeable difference when using only the LLL or including higher Landau levels[27] (as was already noted in Refs. 13 and 28), the LLL approach is used in order to reach higher angular momenta. Vortices can be recognized as points at which the phase jumps by 2π when one walks in a small circle around them (the $0\rightarrow 2\pi$ jumps are indicated

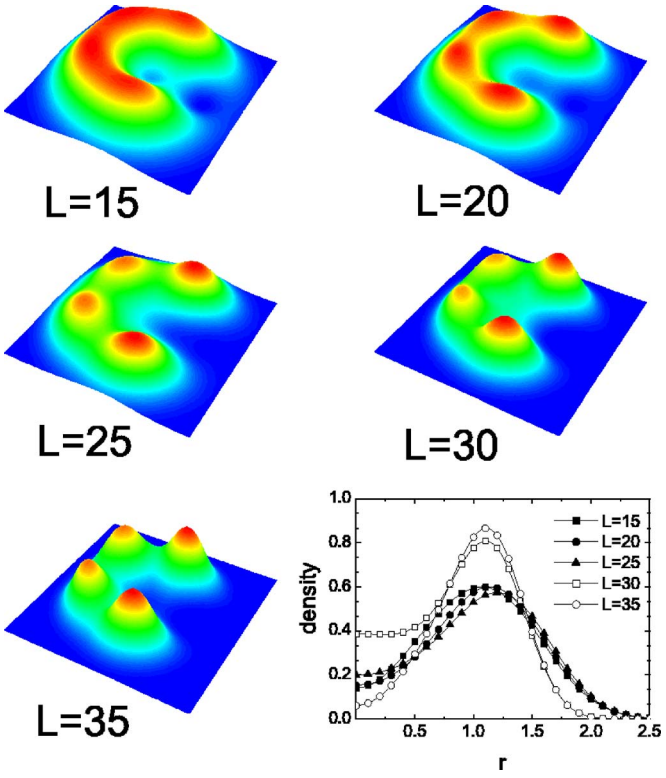

FIG. 6. (Color online) Pair-correlation functions for several ground states at $\lambda=1$ and Ω_c for which this state is the ground state for $N=5$. The angular momentum is indicated next to the plots. Notice how a Wigner crystal forms. The plot in the bottom right corner shows the electron density as a function of r, the distance from the center of the dot, for several ground states.

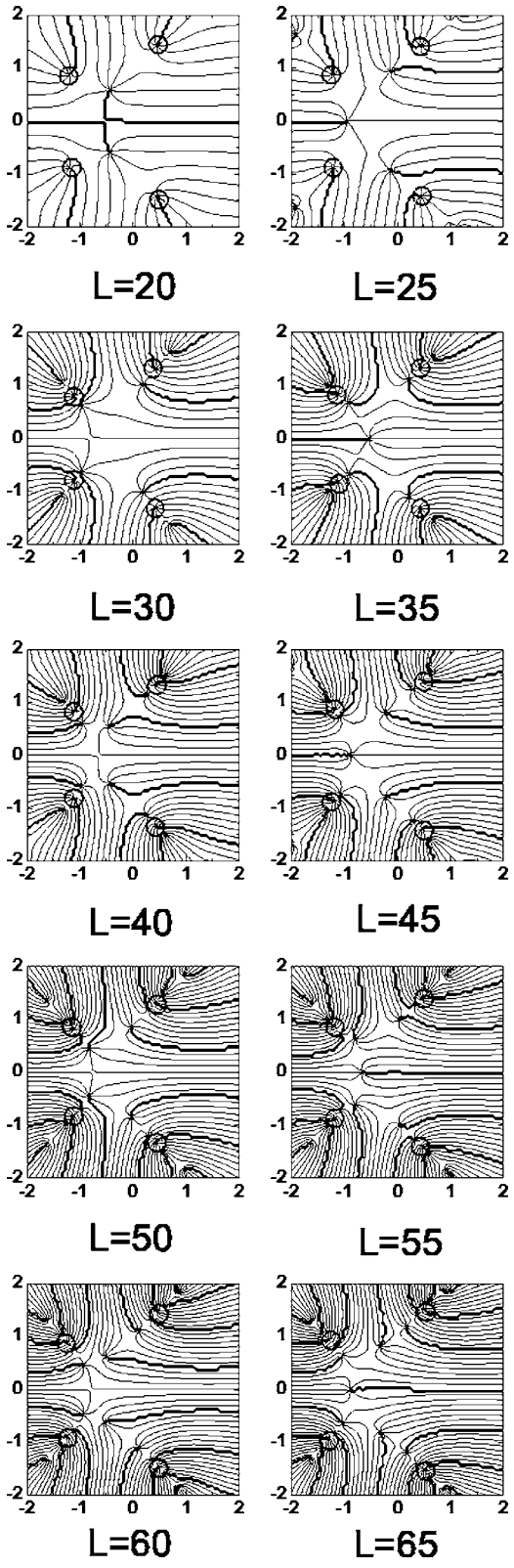

FIG. 7. The phase of the reduced wave function for a system of five electrons for angular momenta ranging from 20 to 65. The $N-1=4$ electrons are fixed on the corners of a pentagon and indicated by the small circles. The thick curves indicate the locations at which the phase jumps by 2π. The vortices are located at the end points of those lines.

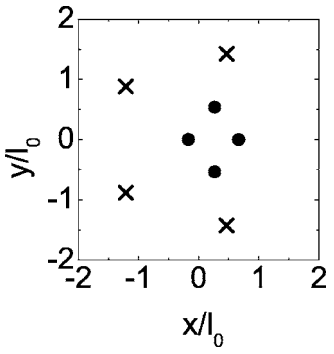

FIG. 8. The locations of the vortices in a system with $N=5$ as calculated with the REM wave functions for the $L=30$ state. The fixed electrons are indicated with crosses and the free vortices with dots. Distances are measured in units of l_0. Notice how the vortices do not cluster around the fixed electrons.

by the thick curves). The electrons are fixed on the corners of a pentagon with a radius obtained by maximizing $|\Psi(\mathbf{r}_1,\ldots,\mathbf{r}_N)|^2$, the squared norm of the multiparticle wave function. The rule that was previously found[29] for $N=3$ and 4 also applies in this case. Every time one goes to the next fully polarized state (i.e., L increases by 5), five vortices are added to the system. One of them enters inside the pentagon, while the four remaining ones settle outside the pentagon (not all vortices outside the pentagon are shown in the figures) on rays from the center. The vortices inside the pentagon tend to adapt their positions to the symmetry implied by the fixed electrons. Notice how, from $L=30$ ($\nu=1/3$) on, the vortices approach the fixed electrons, i.e., they become attached to the electrons. At $L=50$ ($\nu=1/5$) each fixed electron has four vortices in its neighborhood, which move closer to the electron as the angular momentum increases further. After $L=50$ the attached vortices will continue to approach the fixed electrons while new vortices are added inside. Notice that the four vortices that are attached to the electron are localized on a straight line passing through the position of the electron. When these results are compared to the REM result shown in Fig. 8 one notices that in the REM case the vortices do not cluster around the fixed electrons.

From the radial densities plotted in Fig. 6 one notices the remarkable fact that the Wigner crystallization of the $L=30$ state seems less pronounced than for the other states (see also Fig. 9), i.e., the density in the center of the dot is the highest for $L=30$ as compared to the other considered L values. This can also be observed from the pair-correlation plots in the same figure. The vortices in this state tend to approach the fixed electrons (see Fig. 7), forming quasiparticles, i.e., composite fermions. Due to this behavior no vortices will be near the center of the dot and the minimum will be less pronounced. All this results in a more liquidlike nature for the $\nu=1/3$ state than for the other states. In Fig. 9 we show the electron density at the center of the quantum dot. Notice the sharp drops at $L=30\rightarrow 35$ and $L=50\rightarrow 55$, which hint clearly at a transition from a liquidlike to a more solidlike state. This is in accordance with the bulk situation, where $L=30$ and 50 correspond, respectively, to $\nu=1/3$ and $1/5$, where the Laughlin incompressible quantum fluid is formed. Notice

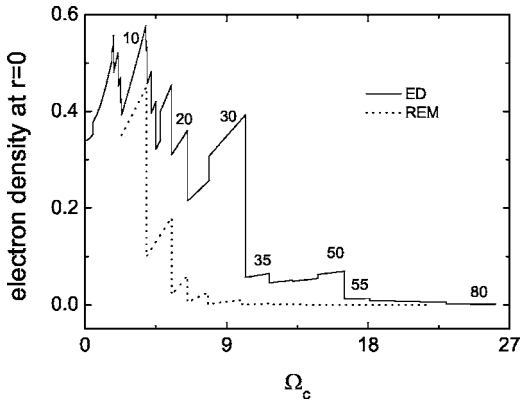

FIG. 9. Electron density at the center of the dot ($r=0$) for the ground state of the $N=5$ system at $\lambda=1$ as a function of the magnetic field. From the $L=20$ state on, the basis functions have been restricted to the LLL. The corresponding REM result (dotted curve) is plotted for L going from 10 to 40. Notice how for the REM case the density drops much faster to zero after the breakdown of the MDD state and fails to show the details of the ED result, i.e., the sudden decrease of the density after $L=30$.

also how for the LLL results ($L=20$ and higher) in Fig. 9 the density at the center of the dot behaves as a straight line as a function of the magnetic field. This is due to the restriction of the basis to the LLL. When we compare the ED results with the REM results plotted in the same figure one can conclude that the REM wave functions overestimate the solidlike behavior of the system as they predict a much faster decrease of the density as a function of the magnetic field. The detailed behavior of the density as calculated with the ED method is not reproduced by the REM calculation; in particular the $L=30$ and 50 states do not exhibit the liquidlike character the ED method predicts.

IV. RESULTS FOR SIX ELECTRONS

In Fig. 10 the phase diagram is plotted for six electrons, showing the ground state as a function of λ and Ω_c without

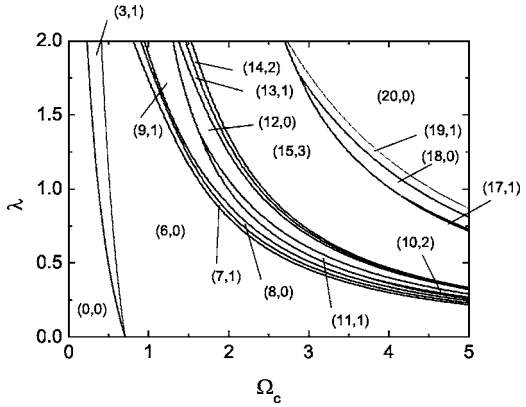

FIG. 10. Phase diagram showing the ground states for a system with $N=6$ electrons as a function of λ and Ω_c. Angular momenta up to 20 are included. The states are indicated as (L,S). Zeeman interaction is not included.

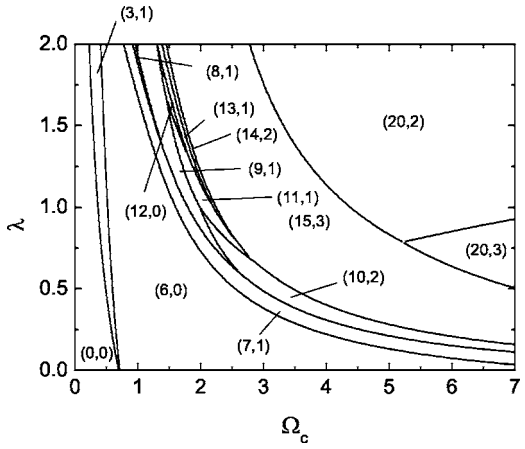

FIG. 11. Same as Fig. 10 but now with Zeeman interaction included.

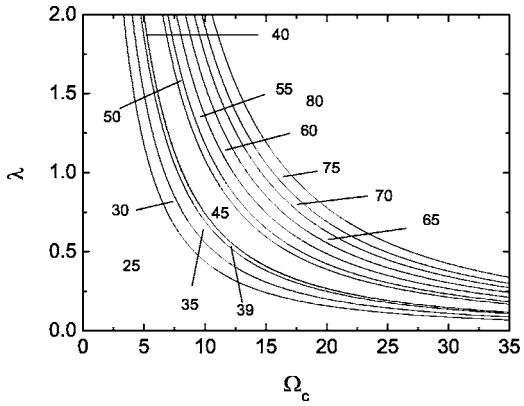

FIG. 12. The ground state at high magnetic fields. Full polarization of the spin was assumed and the exact diagonalization was limited to the LLL. Angular momenta from 25 to 80 are included in the calculation. A very thin area between the $L=39$ and 45 states exists with angular momentum $L=40$, which is almost invisible in this graph.

Zeeman interaction. Figure 11 shows the same but now with Zeeman interaction included, i.e., $g^*=-0.44$. At low magnetic fields the ground state is (0,0) which then is transformed into (3,1) and subsequently (6,0), which is the unpolarized MDD state for six electrons, when the magnetic field increases in strength. If the magnetic field increases further the system transforms into the polarized MDD state (15,3) through a series of closely spaced transitions. As for the system of five electrons, the critical field needed for the transitions $(0,0)\rightarrow(3,1)\rightarrow(6,0)$ depends only slightly on λ since the nature of these transitions is the same as explained in Sec. III but now two electrons need to jump from the first Landau level to the LLL, resulting in two separate transitions. The first transition will be more dependent on λ than the second one due to the fact that one of the electrons already made the jump. Note that in the limit of $\lambda\rightarrow 0$ these two electrons will jump together. Again it can be shown that all the transitions up to the MDD state will happen at some finite value of Ω_c for $\lambda\rightarrow 0$ when the Zeeman interaction is included. This also means that for the case without Zeeman interaction the transition curves will asymptotically approach the $\lambda=0$ line as $\Omega_c\rightarrow\infty$.

Figure 12 shows the ground state as a function of λ and Ω_c for large angular momenta. Due to the long calculation times these were restricted to the LLL and full polarization was assumed. Notice how the state with angular momentum 39 is part of the ground-state sequence. This possibility can also be inferred from the magic angular momentum theory,[16] which predicts that states with $L=15+k\times 5$ can be ground states for a 5-1 symmetry and states with $L=15+k\times 6$ can be ground states for a 6-0 symmetry if the system is fully polarized, with k an integer number. From a calculation with classical particles[15] we know that the two configurations have energies that are very close to each other. By evaluating $|\Psi(\mathbf{r}_1,\ldots,\mathbf{r}_N)|^2$ one is able to determine the symmetry of all states in this phase diagram. The symmetry of most states is clearly predicted, but for the $L=45$ state a mixture of both symmetries emerges. The dominating contribution will be 5-1, with the 6-0 being about half as probable (while for the other states the difference in probability is much larger). The next state that can have both 5-1 and 6-0 symmetry is $L=75$ for which the fivefold symmetry is preferred, with the sixfold symmetry about 24 times smaller in probability (which is still large compared to the other states, which differ by typically a factor 10^{32}). In Ref. 14 the evolution of the system was investigated using a multicenter variational basis. The breakdown of the MDD state and the crossover between the 5-1 and 6-0 symmetries were identified at $\Omega_c=3.05$ and 4.03, respectively, at $\lambda=1.91$, expressed in the units used in the present work. Due to the semiclassical character of the model in Ref. 14 the crossover happens only once, in contrast to the results obtained in the present work. In our "exact" approach we found the MDD breakdown at $\Omega_c=2.72$ at $\lambda=1.91$.

Figure 11 agrees with Fig. 2 of Ref. 9 where γ in Ref. 9 is inversely proportional to our λ.

Information about the symmetry of the ground state can be obtained by investigating the pair-correlation function. Figure 13 shows the pair-correlation function for several ground states of the system. Notice how the symmetry of the state changes with increasing L and how a Wigner crystal forms (see also Fig. 14). The mixture of the 5-1 and 6-0 symmetries for $L=45$ can be observed from the figure as resulting in a smaller probability to find an electron in the center of the quantum dot.

After we obtain the information about the symmetry of the states we are able to fix $N-1$ electrons at the most probable positions and look at the reduced wave function. Figure 15 shows the phase of the remaining wave function for several angular momenta ground states at which the system is fully polarized. The calculations were done in the LLL. The rule that applied previously is now slightly changed since there are two sequences of magic angular momenta. For the sequence corresponding to the 6-0 symmetry the same rule still applies. Each time one reaches the next magic angular momentum one vortex is added inside the polygon of fixed electrons and five are added outside, which happens five times before reaching the $\nu=\frac{1}{3}$ state ($L=45$). For the sequence with 5-1 symmetry each time one reaches the next magic angular momentum, one vortex is added inside the

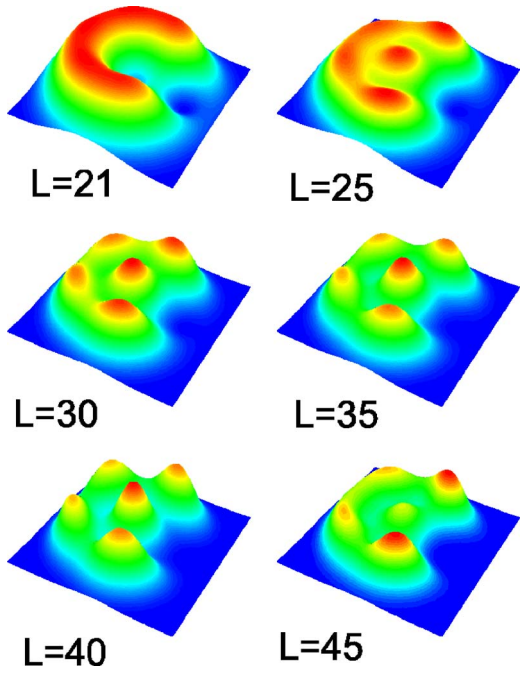

FIG. 13. (Color online) Pair-correlation functions for several ground states at $\lambda=1$ and Ω_c for which this state is the ground state. The angular momentum is indicated next to the plots. Notice how a Wigner crystal forms.

polygon of fixed electrons and four are added outside. This happens six times before reaching the $\nu=\frac{1}{3}$ state ($L=45$) since the electron that is fixed in the center needs two vortices before each electron has two vortices associated with it. The vortices between the fixed electrons always tend to adapt their positions so as to fit with the external symmetry.

In Fig. 12 the $\nu=\frac{1}{3}$ ($L=45$) state is clearly more stable than the other states in the phase diagram. A similar observation can be made for the $N=5$ case ($L=30$) in Fig. 4. In both cases the fixed electrons and the free vortices form composite fermions, as can be seen from the corresponding plots of the phase of the reduced wave function. These states ob-

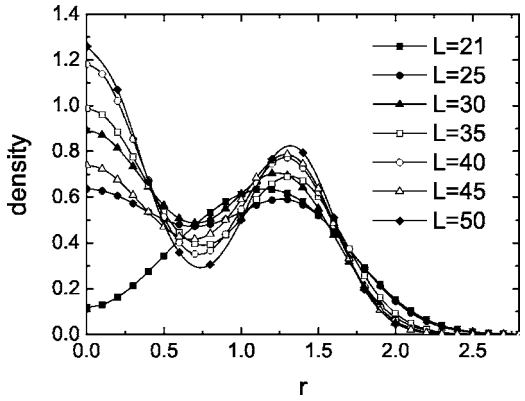

FIG. 14. Radial electron densities as a function of r, the distance from the center of the dot, at $\lambda=1$ for several ground states. The distance is measured in units of l_0. Notice how a maximum forms in the electron density for the states with 5-1 symmetry and how a minimum forms for those with 6-0 symmetry ($L=21$).

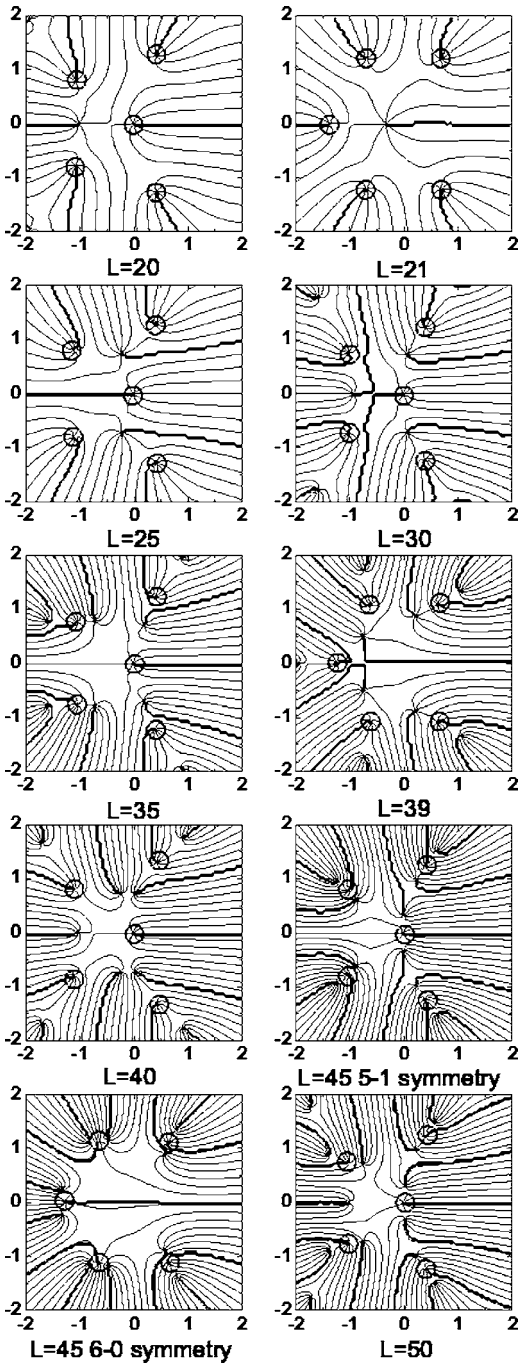

FIG. 15. The phase of the reduced wave function for a system of six electrons for angular momenta ranging from 20 to 50. The $N-1=5$ electrons are fixed on the most probable positions and indicated by the small circles. The thick curves indicate the locations in which the phase jumps by 2π. The vortices are located at the end of these curves. For $L=45$ both the 6-0 and 5-1 symmetries are shown.

tain a higher compressibility since there are no free vortices that can restrict the movement of the electrons toward the center of the dot when the magnetic field is increased. In other words, due to the formation of a composite fermion the $\nu=\frac{1}{3}$ state transforms into an effective $\nu^*=1$ state, forming a MDD-like state, but for the composite fermions and therefore yielding a higher stability. This is also suggested by

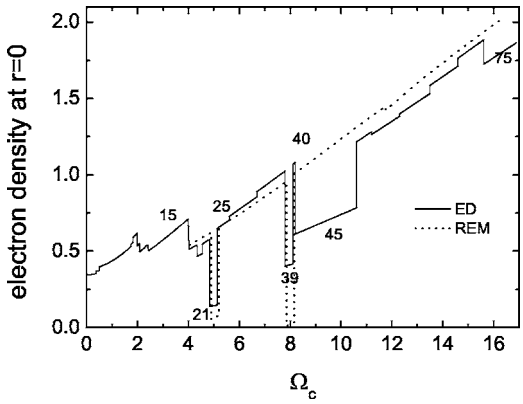

FIG. 16. Electron density at the center of the dot ($r=0$) for the ground state of the $N=6$ system at $\lambda=1$ as a function of the magnetic field. From the $L=25$ state on, the basis functions have been restricted to the LLL. The corresponding REM result (dotted curve) is plotted for L going from 20 to 55. Notice how for the REM case the density increases almost linearly but fails to capture the details of the ED result, i.e., the drop in the density at $L=45$.

formally interpreting $L^*=L-pN(N-1)$ with p defined as in Eq. (1) (in the case of $\nu=\frac{1}{3}$ we have $p=1$) where L^* stands for the angular momentum of the composite fermions.[30] This latter equation is equivalent to $\nu=\nu^*/(2p\nu^*\pm1)$, which clearly shows how $\nu^*=1$ appears. For the $\nu=\frac{1}{5}$ state a similar argument could be considered but due to the spatial extent of the $\nu=\frac{1}{5}$ composite fermion ($L=50$) (see Fig. 7) the effect will probably be minimal or nonexistent, which agrees with the observation in the phase diagrams.

Figure 16 shows the electron density at the center of the quantum dot as a function of the magnetic field. Notice that the behavior is very different from the $N=5$ case (Fig. 9) due to the extra electron, which will cause the density in the center to increase instead of decreasing when the magnetic field increases. At $L=21$ and 39 the density suddenly drops, which corresponds to the 6-0 phase. At $L=45$ there is again a remarkable drop, which originates from the formation of composite fermions, making the state less Wigner-crystal-like as explained before. At $L=75$ a small decrease in density can be observed which corresponds to the $\nu=1/5$ composite fermion formation. The REM results, which are plotted in Fig. 16 by the dotted curve, exhibit a similar behavior to the ED results. The drops in the density at $L=21$ and 39 correspond to the 6-0 phase and are reproduced approximately by the REM results. The REM results, however, fail to reproduce the drop in the density at $L=45$ and to a lesser extent $L=75$, which originate from the formation of the composite fermion at $\nu=1/3$ and $1/5$. From contour plots of the phase of the reduced wave function we know that in the REM calculations the vortices do not approach the fixed electrons. This is, however, the case for the ED calculations. We interpret this discrepancy between the REM and ED results in Fig. 16 as the inability of the REM to describe composite fermion formation.

V. CONCLUSIONS

In Ref. 21 a similar system was investigated using both a spin-density-functional theory (SDFT) technique and an ED scheme. The ED scheme, using a restricted wave function, yields results very similar to the ones presented in this paper; however, the SDFT calculation predicts how the vortices crystallize into a classical point charge distribution. The SDFT results did not give any composite fermion formation and the question remains how to combine these two views. The same system was investigated in Ref. 22, in which the vortices were forced to reveal themselves by breaking the circular symmetry of the system using an elliptic or rectangular potential.

We performed a detailed study of the phase diagram showing the ground-state configuration as a function of the interaction parameter λ and the magnetic field Ω_c for both small and large fields. At small fields the system exhibits a rich structure and several features were explained. At large fields, after the breakdown of the MDD state, the system will follow the angular momentum sequence, which for $N=6$ will yield a competition between the 6-0 and 5-1 symmetries. We found the $L=39$ state appearing in the ground-state sequence (as will $L=21$) and that for the $L=45$ state the 5-1 symmetry is preferred with the 6-0 being half as probable. A comparison with the REM results shows that the latter tends to overestimate the "crystal-like" behavior of the system and fails to capture all the details as shown in the plots of the density at $r=0$. At large magnetic fields some states $\left(\nu=\frac{1}{3}\right)$ appear to be more stable than other states. By investigating the vortex structure this could be explained and an intuitive argument was given: it is due to the vortices approaching the electron and forming a composite fermion. These new particles can be compressed better since they are not hampered by any free vortices still in the system. For the $\nu=\frac{1}{5}$ states a similar behavior was observed, but the effect is much smaller than for $\nu=\frac{1}{3}$. A clear correspondence between the radial density, the vortex structure, and the compressibility was observed. The states without unbound vortices exhibit a better compressibility due to the more liquidlike behavior. It is clear that the clustering of vortices around the fixed electrons, i.e., the formation of composite fermions, is a crucial phenomenon in quantum dots and is closely related to the formation of composite fermions in the fractional quantum Hall effect. The REM theory fails to describe this clustering and therefore also the increased liquidlike behavior of the $\nu=\frac{1}{3}$ state.

ACKNOWLEDGMENTS

This work was supported by the Flemish Science Foundation (FWO-Vl) and the Belgian Science Policy. Fruitful discussions with B. Szafran and T. Stopa are gratefully acknowledged.

*Electronic address: maarten.tavernier@ua.ac.be
†Electronic address: egidijus.anisimovas@ua.ac.be
‡Electronic address: francois.peeters@ua.ac.be

[1] D. C. Tsui, H. L. Stormer, and A. C. Gossard, Phys. Rev. Lett. **48**, 1559 (1982).
[2] R. B. Laughlin, Phys. Rev. Lett. **50**, 1395 (1983).
[3] J. K. Jain, Phys. Rev. Lett. **63**, 199 (1989).
[4] J. K. Jain, Phys. Rev. B **41**, 7653 (1990); **42**, 9193(E) (1990).
[5] *Composite Fermions: A Unified View of the Quantum Hall Regime*, edited by O. Heinonen (World Scientific, Singapore, 1998).
[6] P. A. Maksym, H. Imamura, G. P. Mallon, and H. Aoki, J. Phys.: Condens. Matter **12**, 299 (2000).
[7] L. P. Kouwenhoven, D. G. Austing, and S. Tarucha, Rep. Prog. Phys. **64**, 701 (2001).
[8] S. M. Reimann and M. Manninen, Rev. Mod. Phys. **74**, 1283 (2002).
[9] S.-R. Eric Yang, A. H. MacDonald, and M. D. Johnson, Phys. Rev. Lett. **71**, 3194 (1993).
[10] S. A. Mikhailov, Phys. Rev. B **65**, 115312 (2001).
[11] S. A. Mikhailov and N. A. Savostianova, Phys. Rev. B **66**, 033307 (2002).
[12] S. A. Mikhailov, Phys. Rev. B **66**, 153313 (2002).
[13] S. Siljamaki, A. Harju, R. M. Nieminen, V. A. Sverdlov, and P. Hyvonen, Phys. Rev. B **65**, 121306(R) (2002).
[14] B. Szafran, S. Bednarek, and J. Adamowski, Phys. Rev. B **67**, 045311 (2003).
[15] V. M. Bedanov and F. M. Peeters, Phys. Rev. B **49**, 2667 (1994).
[16] W. Y. Ruan, Y. Y. Liu, C. G. Bao, and Z. Q. Zhang, Phys. Rev. B **51**, 7942 (1995).
[17] A. Matulis and F. M. Peeters, J. Phys.: Condens. Matter **6**, 7751 (1994).
[18] E. Anisimovas and A. Matulis, J. Phys.: Condens. Matter **10**, 601 (1998).
[19] C. Yannouleas and U. Landman, Phys. Rev. B **66**, 115315 (2002).
[20] C. Yannouleas and U. Landman, Phys. Rev. B **68**, 035326 (2003).
[21] H. Saarikoski, A. Harju, M. J. Puska, and R. M. Nieminen, Phys. Rev. Lett. **93**, 116802 (2004).
[22] H. Saarikoski, S. M. Reimann, E. Rasanen, A. Harju, and M. J. Puska, Phys. Rev. B **71**, 035421 (2005).
[23] Gun Sang Jeon, Michael R. Peterson, and J. K. Jain, Prog. Inorg. Chem. **72**, 035304 (2005).
[24] A. F. Slachmuylders, B. Partoens, and F. M. Peeters, Phys. Rev. B **71**, 245405 (2005).
[25] P. A. Maksym, Phys. Rev. B **53**, 10871 (1996).
[26] M. B. Tavernier, E. Anisimovas, F. M. Peeters, B. Szafran, J. Adamowski, and S. Bednarek, Phys. Rev. B **68**, 205305 (2003).
[27] The statement is true as long as the fixed electrons are situated on, or near, their most probable positions as was done in Figs. 7 and 15. As was shown in Ref. 29 in certain configurations antivortices can form, which cannot be described by using the LLL approximations due to the polynomial character of the LLL wave functions.
[28] A. D. Guclu and C. J. Umrigar, Phys. Rev. B **72**, 045309 (2005).
[29] M. B. Tavernier, E. Anisimovas, and F. M. Peeters, Phys. Rev. B **70**, 155321 (2004).
[30] Chia-Chen Chang, Gun Sang Jeon, and J. K. Jain, Phys. Rev. Lett. **94**, 016809 (2005).